CALIBRATION AND PROCESSING CONSTRAINTS ON ANTENNA AND FEED DESIGNS FOR THE SKA: I

ATHOL KEMBALL[1,2], TIM CORNWELL[3], AND MARK YASHAR[2]

DEPT. ASTRONOMY[1] & IACAT/NCSA[2] (UNIVERSITY OF ILLINOIS AT URBANA-CHAMPAIGN) & ASKAP PROJECT (AUSTRALIA TELESCOPE NATIONAL FACILITY)[3]

AUGUST 2009

ABSTRACT

This memo considers the constraints posed on antenna and feed designs for the SKA by calibration and processing requirements for the array. The calibration and imaging formalism applicable to the SKA is summarized, with a specific focus on direction-dependent calibration effects of relevance to reflector and feed designs. The general issue of overall SKA system design optimization is discussed as it applies to performance trade-offs between hardware and downstream calibration and processing design technologies. Initial, zeroth-order constraints on array performance, expressed in simple antenna and feed parameters, are derived from imaging dynamic range requirements for the SKA. A detailed discussion of antenna and feed design constraints posed by computational cost considerations is deferred to a separate memo.

INTRODUCTION

At the highest level, the overall system design for the SKA has to meet the transformative science goals of the telescope, be technically feasible, and fall within the overall cost envelope set for the project. In a simple linear idealization of the system design process for the SKA, depicted as a waterfall model in Figure 1, the science requirements translate to technical specifications; these, in turn, are expressed as a reference technical design composed of design technology choices over multiple sub-systems. The component design technologies are strongly coupled in many instances, both where they interface directly to one another, but also as part of performance and cost trades within the overall system design optimization. For the SKA, the antenna and feed design is coupled in both senses to calibration and processing design technology choices. The high cost and feasibility requirements on calibration and processing posed by the SKA wide-field imaging and non-imaging science goals make this coupling more visible and noteworthy for the SKA, but indeed such trade-offs been present historically in the design decisions made for all radio interferometers, as we will illustrate in further detail below. In addition, calibration and processing constraints may act also as explicit design drivers for the SKA, by restricting or excluding the range of engineering choices that

can be made. For example, certain array designs may have computing costs that exceed an affordable fraction of the total project cost envelope.

The scientific performance of radio interferometers can be assessed against a simple high-level metric: are their final science products (either imaging or non-imaging) limited only by the inherent sensitivity of the array ? Equivalently, is the noise floor in the final science products defined by the thermal noise limit, σ_{th}, derived from the system equivalent flux density (SEFD) or A/T, over plausible integrations in bandwidth and time, or is a higher barrier set by *uncorrected* systematic errors ?

For imaging applications, if the peak brightness in an image field is denoted by S_m, then the target thermal dynamic range is:

$$DR_{th} = \frac{S_m}{\sigma_{th}} \sim S_m \frac{\sqrt{2\,\Delta t\,\Delta f}}{SEFD}\eta \tag{1.1}$$

where Δt is the integration interval over time, Δf is the bandwidth, and η ~ O(1) is a scaling factor for digitization or signal processing effects. In practice, this dynamic range limit will not be achieved if the data are corrupted by *uncorrected* systematic errors arising from un-modeled propagation or calibration errors along the signal path (conventionally defined as the path between the incident point of the astronomical radiation above Earth's atmosphere to the output of the final instrumental back-end on the array) or by image formation, source model representation, or deconvolution errors. Although they are important, we do not consider the latter three factors here, given the instrumental focus of this memo on calibration and processing constraints that affect antenna and feed design parameters.

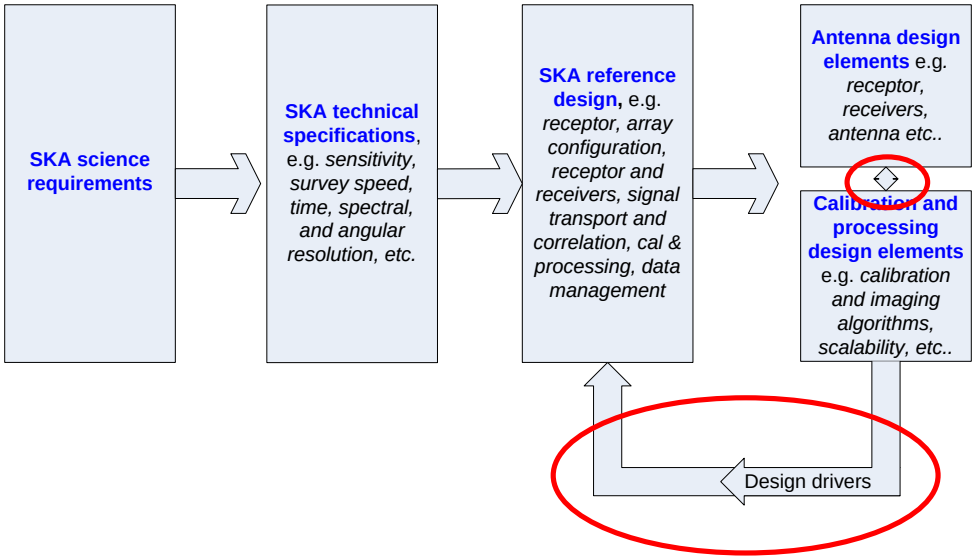

Figure 1. A simplified waterfall depiction of the overall system design process for the SKA. The coupling between antenna design elements and calibration and processing design elements is shown explicitly, as is their role as potential design drivers.

Systematic instrumental errors do not integrate down in a $\sqrt{N}$ sense; they compromise the achieved level of residual noise and change its distribution to non-Gaussian form in a manner that is

rarely analytically tractable. For imaging applications of the SKA, the image products will be dynamic-range limited in this case.

Clearly, the key issue is the extent to which these errors are *uncorrected*, i.e. how effectively are they removed or mitigated by the upstream hardware design of the array or the downstream calibration and processing technologies. This performance trade-off defines the crux of system design optimization for any radio interferometer, but is especially acute for the SKA. Targeted continuum deep field imaging may require a dynamic range of 70 dB (Schilizzi et al. 2007) or up to 85 dB (Condon 2009). Historical precedent with existing radio interferometers suggests very strongly that investment in upstream hardware performance is the preferred method of mitigating instrumental errors. This statement is made with full awareness, however, that cost curves frequently rise very sharply close to current engineering design limits and that upstream hardware optimization is constrained by cost-effectiveness.

Equally important however, is the understanding that not all instrumental errors can be corrected reliably downstream by calibration and processing. In order to understand this trade-off more clearly, we outline the calibration and imaging problem for SKA in the following section, then consider the simplest constraints this poses on antenna and feed designs.

CALIBRATION AND IMAGING WITH THE SKA

The SKA is defined by its science requirement for high sensitivity, achieved primarily through a large collecting area. Consequently, this requires that the array achieve a very high thermal dynamic range, as defined by the metric in equation (1.1) above. In imaging applications, the SKA also needs to achieve this dynamic range *over a wide field of view*. As a result, this feasibility risk will be strongly (but not exclusively) influenced by instrumental design decisions that have direction-dependence, such as those made for the antennas and feeds.

Wide-field, high dynamic-range imaging with the SKA requires a formalism that includes direction-dependent effects in routine calibration and imaging. Following Hamaker, Bregman, & Sault (1996ff), as generalized to include image-plane effects by Cornwell (1995) and Noordam (1995), we adopt the imaging equation:

$$V_{mn} = \prod_k \left[G_m^k \otimes G_n^{k*} \right] \int_\Omega \prod_k \left[T_m^k(\vec{\rho}) \otimes T_n^{k*}(\vec{\rho}) \right] e^{-2\pi j \vec{b}_{mn} \cdot (\vec{\rho} - \vec{\rho}_s)} K\, S(\vec{\rho}) d\Omega \qquad (1.2)$$

using the nomenclature of Kemball & Martinsek (2005), where V_{mn} is the complex correlation 4-vector measured over all polarization cross-products on array baseline $\vec{b}_{mn}$ (with frequency as an implicit coordinate) and $S(\vec{\rho})$ is the associated 4-vector of image brightness in Stokes parameters $\{I,Q,U,V\}$ toward direction $\vec{\rho}$. The 4 x 4 matrix *K* converts the image brightness from a Stokes $\{I,Q,U,V\}$ basis to the nominally-orthogonal polarization receptor basis (e.g. crossed linear or circular). Antenna-dependent instrumental corrections in the visibility plane are denoted by 2 x 2 Jones matrices G_m^k, where *k* denotes the instrumental correction type, and *m* indicates antenna index. The symbol $\otimes$ denotes an outer matrix product, and $j = \sqrt{-1}$. The image-plane (direction-dependent) calibration terms are denoted by $T_m^k(\vec{\rho})$; these are similarly 2 x 2 Jones matrices and follow the index convention used for visibility-plane corrections. Note that for antennas with primary beam patterns that rotate on the sky during aperture synthesis (e.g. fixed feeds on an azimuth-

elevation antenna mount), the set $T_m^k(\vec{\rho})$ includes a parallactic angle rotation matrix. The calibration terms G_m^k and $T_m^k(\vec{\rho})$ may also be arbitrarily parametrized.

Many existing interferometers adopt an approximate form of the full imaging equation (1.2) during calibration and processing. This may be possible in cases of lower sensitivity (and hence lower target dynamic range) or a narrower field of view than that required by the SKA. Such simplifications may include:

i) An approximation of the integral kernel $\vec{b}_{mn} \cdot (\vec{\rho} - \vec{\rho}_s)$ to reduce it to 2-D Fourier form.

ii) A discrete, unparametrized representation for visibility-plane corrections G_m^k.

iii) Image-plane corrections $T_m^k(\vec{\rho})$ that are assumed constant over time or axisymmetric; this moves these terms outside the integral in (1.2).

These assumptions reduce the imaging equation to a form that allows separable calibration and imaging in conventional form, as:

$$V_{mn}(u,v) = \prod_k \left[G_m^k \otimes G_n^{k*} \right] \int_\Omega S(\eta,\xi)\, e^{-2\pi j(u\eta+v\xi)}\, d\Omega \tag{1.3}$$

using conventional nomenclature for image-plane coordinates (η,ξ) and 2-D *uv*-plane coordinates (u,v) and where the final image may be corrected for mean image-plane effects. The approximations inherent in equation (1.3) will not be possible for SKA-mid, or SKA-lo, and are indeed not possible for precursor telescopes such as the MWA[1] (Mitchell et al 2008), PAPER[2], ASKAP[3], or MeerKAT[4]. Instead we need to consider calibration and imaging within the direction-dependent formalism of equation (1.2).

For calibration and imaging within the imaging equation formalism, we need estimators $\hat{G}_m^k, \hat{T}_m^k,$ and $\hat{S}(\vec{\rho}),$ given the constraints posed by the observed visibility data. All three sets of unknowns need to be solved for on an equal footing, either jointly or iteratively. This is an ill-posed problem, but is assumed regularized and convergent in what follows. In a chi-squared formalism (Cornwell 1995):

$$\begin{aligned} \chi^2 &= \sum_{mn} \left\| V_{mn} - \prod_k \left[G_m^k \otimes G_n^{k*} \right] \int_\Omega \prod_k \left[T_m^k(\vec{\rho}) \otimes T_n^{k*}(\vec{\rho}) \right] e^{-2\pi j \vec{b}_{mn} \cdot (\vec{\rho}-\vec{\rho}_s)} K\, S(\vec{\rho}) d\Omega \right\| \\ \chi^2 &= \Delta V^\dagger W\ \Delta V \\ \Delta V &= V_{mn} - \widehat{V}_{mn},\ \forall\ (m,n) \end{aligned} \tag{1.4}$$

[1] http://www.mwatelescope.org/

[2] http://astro.berkeley.edu/~dbacker/eor/

[3] http://www.atnf.csiro.au/projects/askap/

[4] http://www.ska.ac.za/

where $\hat{V}_{mn}$ is defined by the relation: $\chi^2 = \sum_{mn} \left\| V_{mn} - \hat{V}_{mn} \right\|$ and W in the adopted weighting.

Defining calibration here as the solution for instrumental terms $\hat{G}_m^k$ and $\hat{T}_m^k$, this formalism allows generalized calibration or self-calibration by iteratively fixing $S(\vec{\rho})$ and computing χ^2 at the N positions of unknown calibration Jones matrices in the imaging equation, then solving using nonlinear least-squares methods to find the minimum at: $\frac{\partial \chi^2}{\partial G_m^k} = \frac{\partial \chi^2}{\partial T_m^k} = 0$ (Cornwell 1995; Kemball & Martinsek 2005). A flexible package for parametrized calibration within the imaging equation formalism is provided by MeqTrees[5] (Noordam & Smirnov 2009).

Formation of a dirty image $S_D(\vec{\rho})$ within the formalism of equation (1.2) is can be posed as the update direction for χ^2 at $S(\vec{\rho}) = 0$, incorporating a Hessian normalization (Cornwell 1995):

$$S_D(\vec{\rho}) = \left[\frac{\partial^2 \chi^2}{\partial S(\vec{\rho}) \partial S^T(\vec{\rho})} \right]^{-1} \left. \frac{\partial \chi^2}{\partial S(\vec{\rho})} \right|_{S(\vec{\rho})=0} \tag{1.5}$$

This is an expression of the image formation problem in variational form. Image formation is inherently linear however, and an equivalent formulation is: $d = AS + n$, where d is the measured data, A is a non-square measurement matrix, and n is noise (Cornwell 2008).

It is important to note that image formation plus deconvolution in the presence of *known* direction-dependent calibration errors $T_m^k(\vec{\rho})$ is a *solved problem* within this framework (Bhatnagar et al. (2008); Morales & Matejek (2009)). At the highest level, this is not an open research question for the SKA.

In the following section we consider the implication of these requirements on calibration and imaging on SKA design optimization.

IMPLICATIONS FOR SKA DESIGN OPTIMIZATION

The overall SKA design optimization problem described in the Introduction requires trade-offs between the cost and performance of upstream hardware components versus downstream calibration and processing solutions to correct for any residual instrumental response. There is a school of thought that this hardware optimization should proceed independently of any downstream calibration and processing considerations. In this approach, it is the task of calibration and processing to remove any residual instrumental errors, whatever they may turn out to be, and that the best antenna and feed for SKA is the one that can be extrapolated cost-effectively from existing hardware designs. This argument is frequently reformulated as an antenna and feed design optimization that produces the largest collecting area for the lowest cost. While this argument simplifies and decouples the SKA system design process, which is a significant advantage, it is unfortunately not sufficient if we are to ensure that the SKA meets its wide-field imaging science

[5] http://www.astron.nl/meqwiki/MeqTrees

goals. The imaging and sensitivity requirements of the SKA are demanding, and represent an extrapolation over several orders of magnitude from the current state of practice in radio interferometry. A systems design is essential, incorporating all constituent technologies in a joint optimization, using a metric tied to the final science product (e.g. achieved wide-field imaging dynamic range). We cannot afford to design an array that cannot be calibrated to the specifications required for SKA science.

Not all downstream instrumental effects can be reliably calibrated and removed from the observed array data. This is especially true for instrumental errors for which any or several of the following factors are true:

a) ***High-order parameterization:*** Numerically stable, robust, and convergent solvers are proportionally more difficult to develop for calibration terms that require a large number of free parameters to model accurately; this is especially true at low S/N.

b) ***Strong time-variability:*** Instrumental effects that are vary over time constitute a special case of (a) if the time-variability can be modeled with additional parameters, but if insufficiently stable this can render the calibration infeasible. In addition, terms that are discontinuous over time or frequency pose special challenges.

c) ***No parametric model:*** Calibration terms that have a parametric model that can be derived from an underlying physical model are generally easier to solve for than terms with a purely empirical model.

d) ***Poor constraints:*** Instrumental calibration errors that are poorly constrained by the observed data may not be solvable. For example, it may be difficult to solve for direction-dependent effects at positions in the primary beam where there are no sufficiently bright calibration sources.

e) ***Non-separable:*** Instrumental calibration terms that cannot be solved for in a separable manner from other instrumental errors introduce greater complexity (and perhaps instability) into the calibration process.

f) ***Non-Gaussian statistics:*** Any processes that introduce non-Gaussian noise into the data stream are proportionally more difficult to address, e.g. RFI.

g) ***Large absolute value:*** Calibration errors that have a large absolute value relative to the thermal noise limit, and are not easily removed, complicate the calibration process and may limit the final achieved dynamic range through simple propagation of fractional calibration errors.

h) ***High computational cost:*** Calibration terms that require high computational costs or complex algorithms to remove pose cost and implementation risks.

As a simple example of calibration risks and hardware-software trade-offs, consider direction-dependent (non-isoplanatic) calibration errors, denoted by $T_m^k(\vec{\rho})$ in the discussion in the previous section; specifically those introduced by the primary beam voltage pattern at appreciable distances from the optical axis. Pointing errors are a zeroth-order element of this instrumental error. It is instructive to consider how these errors are currently handled by existing interferometers in wide-field imaging observations. The VLA has a polarization beam squint and an alt-az antenna mount; in contrast the WSRT has an equatorial mount. High dynamic-range wide-field imaging with the VLA accordingly requires a correction for the primary beam as it rotates on the sky over the

course of the observation, incorporating beam squint. This instrumental effect, when compared to routine amplitude calibration for example, meets many of the special conditions enumerated above. As a result, despite the fact that the VLA has been in operation for almost 30 years, these effects have only recently been removed (e.g. Bhatnagar et al. 2008), and stable interferometric solvers for the primary beam response are an important contemporary research topic. In contrast, WSRT has generally achieved higher wide-field dynamic range than the VLA in L-band imaging; a strong argument can be made that this is aided by its antenna mount and feed choice.

The high target thermal dynamic range for the SKA requires automated routine calibration at a level exceeding current practice, both in terms of the range of instrumental effects removed (e.g. direction-dependent terms), but also in regard to the accuracy of the calibration required. As a result, it is important for the SKA to minimize the general calibration risk factors enumerated above in (a) through (h), and the most effective means to do this is through upstream hardware optimization as part of an overall system design optimization. Advances in current algorithmic approaches for dealing with direction-dependent calibration are summarized in a recent paper by Bhatnagar (2009); this algorithmic work will need to continue for SKA, as a joint design optimization of both hardware and calibration and processing technologies will be needed

We note also as part of this section that there is a significant difference between *solving* for unknown SKA instrumental errors, and *applying* pre-existing calibration terms. This is especially true for direction-dependent instrumental calibration, for which many of the general calibration risk factors listed earlier in this section hold true. Known instrumental corrections $\hat{G}_m^k$ and $\hat{T}_m^k$ can readily be applied during image-formation using equation (1.5), as noted above, as long as the calibration terms are known to sufficient accuracy. We will discuss the latter condition in further detail below. However, their solution in equation (1.4) is a more challenging and less constrained problem. These issues hold true for the SKA considered either as a pointed PI-driven instrument, or as a survey telescope with scheduled calibration observations. Undoubtedly, however, these problems can be better controlled in the latter operational mode, as by applying a priori corrections in real-time, the residual calibration problem becomes second-order.

In the following section, we derive simple zeroth-order constraints on antenna and feed design parameters based primarily on imaging fidelity considerations and the calibration issues discussed above.

IMPLICATIONS FOR ANTENNA AND FEED DESIGN PARAMETERS

Focusing on the specific sub-problem of antenna and feed design optimization, the calibration and processing issues we must address as part of the trade-off between hardware design and calibration and processing technologies primarily (but not exclusively) concerns issues related to the feasibility and cost of image-plane (direction-dependent) calibration and imaging, i.e. they relate to the primary beam response pattern, antenna diameter, mount type, and related parameters.

In order to derive zeroth-order constraints on these antenna and feed design parameters, we apply a simple error propagation analysis to the image formation process. This underlying approach was first used for general interferometric mosaicing array design optimization by Cornwell et al. (1993).

For the SKA our image-formation process is defined by equation (1.5). Neglecting the normalization factor, the image formation equation reduces to the form (Cornwell 1995):

$$S_D(\vec{\rho}) = \left.\frac{\partial \chi^2}{\partial S(\vec{\rho})}\right|_{S(\vec{\rho})=0} = -2\,\mathrm{Re}\sum_{mn} X_{ij}^{*T}(\vec{\rho})\, W_{mn}\, V_{mn}^{obs}$$

$$X_{ij}^{*T}(\vec{\rho}) = \prod_k \left[G_m^k \otimes G_n^{k*} \right] \int_\Omega \prod_k \left[T_m^k(\vec{\rho}) \otimes T_n^{k*}(\vec{\rho}) \right] e^{-2\pi j \vec{b}_{mn}\cdot(\vec{\rho}-\vec{\rho}_s)} K\, S(\vec{\rho}) d\Omega \tag{1.6}$$

For this initial memo, we derive zeroth-order constraints by simplifying the image formation process to the case of: i) single polarization scalar calibration; ii) a high level of completeness in *uv*-coverage (which is a reasonable assumption for the SKA); iii) equatorially-mounted antennas and feeds (fixed on the sky); iv) uniform weighting; and v) a target field with an offset, single unit-brightness point-source component $S(\vec{\rho}) = \delta(\vec{\rho} - \vec{\rho}_s)$. The latter is a particularly poor assumption for SKA image fields, but it a useful assumption for investigating the degradation of imaging fidelity as a function of radial distance from the optical axis in our initial coarse analysis here. In this simplification, the observed visibility data V_{mn}^{obs} contain the effect of the true instrumental effects $\{G_m^k, T_m^k(\vec{\rho})\}$ acting on the adopted source model $S(\vec{\rho}) = \delta(\vec{\rho} - \vec{\rho}_s)$ via equation (1.2), and $X_{ij}^{*T}(\vec{\rho})$ (in equation (1.6)) contains the actual applied calibration corrections $\{G_m^{'k}, T_m^{'k}(\vec{\rho})\}$, where $\{G_m^{'k}, T_m^{'k}(\vec{\rho})\} \neq \{G_m^k, T_m^k(\vec{\rho})\}$ in practice. We seek to understand the impact on dynamic range of these calibration errors, parametrized here in terms of simple antenna and feed design parameters.

For our initial simplifying assumptions:

$$S_D(\vec{\rho}_s) = -2\,\mathrm{Re}\sum_{mn}\left[T_m^{'k}(\vec{\rho}_s) \otimes T_n^{'k*}(\vec{\rho}_s) \right]^{*T} \left[T_m^k(\vec{\rho}_s) \otimes T_n^{k*}(\vec{\rho}_s) \right]$$

or (1.7)

$$S_D(\vec{\rho}_s) = -2\,\mathrm{Re}\sum_{mn}\left[G_m^{'k} \otimes G_n^{'k*} \right]^{*T} \left[G_m^k \otimes G_n^{k*} \right]$$

We consider the variance in the image (assumed to be $S_D(\vec{\rho})$ at the point-source position $\vec{\rho}_s$), equivalently expressed as the inverse squared dynamic range limit, by a simplified error propagation analysis for each calibration error term $q \in \{G_m^k, T_m^k(\vec{\rho})\}$ considered individually.

$$DR^{-2} = \sigma^2_{S_D(\vec{\rho})} \sim \left(\frac{\partial S(\vec{\rho})}{\partial q} \right)^2 \sigma_q^2 \tag{1.8}$$

where σ_q^2 is the residual variance in each calibration term *after correction.* In this sense it is the net residual after hardware and calibration optimization as described above. All dynamic range expressions in what follows should be read in that sense. Also, in the summation over baseline index *mn* in equation (1.8), we will make the further simplification that we are considering a single calibration interval, and that standard errors decline statistically as $\sqrt{N}$, which is $\sim N_a^{-1/2}$ in this instance, where N_a is the number of antennas in the array. For multiple visibility integrations per common calibration solution interval a further scaling by the square root of this interval multiple is required (see factor *M* in Perley (1986)).

Amplitude and phase errors – If we assume a visibility-plane amplitude calibration error term of the form $G_m = (1+\gamma)e^{j0}$, with zero phase and a real amplitude deviation γ from a true value of unity, then:

$$DR \sim \frac{\sqrt{N_a}}{\sigma_\gamma} \tag{1.9}$$

A similar analysis (and relation) holds for phase errors. The influence of amplitude and phase errors of this type on image dynamic range was first considered by Perley (1986) using an approach including basic deconvolution; however the results here are consistent with the earlier expressions but differ by a scaling factor $\sqrt{N_a}$ due to differing assumptions of statistical dependence. Condon (2009) applied the Perley (1986) relations to the case of general calibration of the SKA.

These relations can be applied broadly to all types of amplitude and phase errors in the system, including, for example, uncertainties in the bandpass response function amplitude or phase.

Pointing errors – We assume a primary beam response function of simple Gaussian form with amplitude $e^{-\frac{(\rho-\rho^0)^2}{\alpha^2}}$, neglecting phase, where ρ is the angular separation from the optical axis, ρ^0 is the pointing error from the nominal pointing position, and the FWHM is $\alpha\sqrt{2\ln 2}$. If the pointing errors for each antenna *m*, denoted ρ_m^0, are considered statistically independent, and drawn from a common normal zero-mean marginal distribution $N\left(0,\sigma_{\rho^0}^2\right)$, we obtain:

$$DR \sim \sqrt{N_a}\left(\frac{\alpha}{\rho}\right)\left(\frac{\alpha}{\sigma_{\rho^0}}\right) \tag{1.10}$$

Beam-width errors – Assuming the same primary beam shape as used in the pointing error analysis, and adopting an actual FWHM at each antenna *m* of α_m, assumed similarly statistically independent and drawn from a common marginal normal distribution $N\left(0,\sigma_\alpha^2\right)$, results in a dynamic range:

$$DR \sim \sqrt{N_a}\left(\frac{\alpha}{\rho}\right)^2\left(\frac{\alpha}{\sigma_\alpha}\right) \tag{1.11}$$

We note that both equations (1.10) and (1.11) show a significant degradation of dynamic range with increasing angular distance from the field center (assumed here aligned with the feed/antenna optical axis), consistent with practical experience in wide-field imaging with current interferometers.

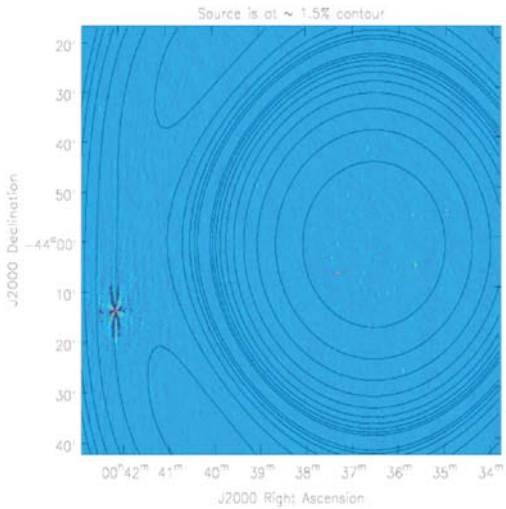

Figure 2. ATCA observations at 1.4 GHz showing artifacts remaining at the position of a source at 1 degree from the pointing center, before correction by a holographic beam response (shown as a contour). After correction fine-scale sidelobes from the confusing source remain distributed across the field, limiting dynamic range (from work by Cornwell and collaborators at ATNF).

Mount type – In this simplified analysis we have considered equatorially-mounted antennas with fixed feeds on the sky (including, to first order, the sky-mounted feed arrays planned for ASKAP using a mechanical feed rotator). We may well ask how the relations (1.12) and (1.13) extrapolate to antenna and feed mounts that rotate on the sky during aperture synthesis; as an example, fixed feeds on azimuth-elevation antenna mounts. As noted above, the parallactic angle rotation of the adopted beam pattern for each antenna is removed as part of the set of direction-dependent corrections $T_m^k(\vec{\rho}_s)$ applied during image formation using equation (1.5). The accuracy of the parallactic angle correction is set by a trading the computational cost against the size of the parallactic angle bin used for the visibility time series during this correction (Bhatnagar et al. 2008). However, we can also reasonably argue that the error in the beam pattern introduced by physical rotation (e.g. changing gravitational deformation) may be broadly comparable to the error at a fixed point in the pattern, as considered above. In this very simplified extrapolation, we can argue that this error will add in quadrature to decrease the dynamic range in equations (1.10) and (1.11) by a factor of $\left[\sqrt{2}, \sqrt{few}\right]$, but with *considerable* uncertainty. In general, arrays with azimuth-elevation antennas have achieved lower dynamic range than equatorially-mounted arrays in practice, roughly by such a factor, but there are multiple causes, including errors introduced by assuming axisymmetric beams and/or no parallactic angle rotation. It is instructive to ask how the discussion of mount type accords with practical experience in high-fidelity wide-field imaging with current interferometers at L-band. As noted above, practical experience shows that the equatorially-mounted WSRT produces higher quality images than contemporary alt-az arrays such as the VLA. This is consistent with the stability of the primary beam response on the plane of the sky over the course of the synthesis in this antenna mount configuration.

Optics and diffractive effects - Even for parabolic antennas, it is difficult to model the full diffractive effects in the antenna response (e.g. feed legs) at the level of fidelity required for the target SKA dynamic range; this is especially true for blocked or partially blocked optics. This issue is coupled to the problem of rotation on the plane of the sky, as discussed in the preceding section on antenna mount type. Practical experience with current deep wide-field observations suggest that these diffractive effects are difficult to remove with high accuracy, due both to their complex angular structure on the sky and dependence on both time and frequency. Middelberg et al. (2008; and

Figure 2) describe deep 1.4 GHz ATCA observations affected by residual artifacts from a strong confusing source at 1 degree from a pointing center used in the survey, even after precise satellite holography to measure the primary antenna sidelobe pattern. It is also not yet clear that detailed electromagnetic antenna modeling presents an alternative approach sufficiently accurate to remove the effects of the antenna primary beam; it would require very accurate modeling of all diffractive structures, and it is possible that practical operational considerations (e.g. moisture, mechanical defects) could detract from the accuracy of an a prior correction for each antenna element. Further work remains to be done in this area, especially with the pathfinder arrays.

FUTURE WORK

This memo has described the calibration and imaging formulation applicable to the SKA and its precursor arrays, with a specific focus on direction-dependent calibration errors which are of special relevance to feed and antenna design. Simple zeroth-order heuristics on feed and antenna design parameters have been presented, derived from constraints on imaging dynamic range. This memo has also considered the overall problem of trade-offs between hardware optimization and calibration and processing optimization, as part of a joint SKA systems design.

However, this introductory memo presents several idealizations as openly stated above. In reality antenna-feed combinations for the SKA will have complex beam patterns and their interaction with realistic low-frequency sky models is needed to examine this problem in much greater detail. In this regard, complementary approaches are needed using both simulation and practical experience acquired from SKA pathfinder arrays such as ASKAP, MeerKAT, ATA, and the EVLA. We also need to understand the extent to which beam patterns can be accurately predicted using electromagnetic modeling for prototype SKA reflector-feed combinations, as verified against holography, and interferometric measurement. Experience with the accuracy of modeled beam response patterns for current arrays is mixed, perhaps due to their design and blockage, but this issue is important given the stringent demands placed by high dynamic range on antenna and feed design parameters. A key question will also be the time-stability and frequency response of the beam patterns over a range of appreciable angular separation from the optical axis.

It is important to note that mitigation is also possible, including imaging fields over a smaller fraction of the main beam (albeit at the cost of survey speed) and confining ultra-deep targeted imaging to less confused fields.

We will consider these issues in subsequent memos in this series, including considerations of computational cost as a constraint on antenna and feed design parameters.

ACKNOWLEDGEMENTS

This material is based upon work supported by the National Science Foundation under Grant No. AST 0431486. Any opinions, findings, and conclusions or recommendations expressed in this material are those of the author(s) and do not necessarily reflect the views of the National Science Foundation.

REFERENCES

Bhatnagar, S. 2009, *"Calibration and Imaging Challenges at Low Radio Frequencies: An Overview of the State of the Art"*, in The Low Frequency Radio Universe, eds. Saikia, Green, Gupta, & Venturi (ASP Conference Series LFRU), in press.

Bhatnagar, S., Cornwell, T.J., Golap, K., & Uson, J.M. 2008, *"Correcting Direction-Dependent Gains in the Deconvolution of Radio Interferometric Images"*, Astro. Astroph., **487**, 419.

Condon, J. 2009, *"Sensitive Continuum Surveys with the SKA: Goals and Challenges"*, presented at the SKA Continuum Imaging Workshop, http://www.ska.ac.za/ska2009/download/ws_condon.pdf

Cornwell, T.J., Holdaway, M.A., and Uson, J.M. 1993, *"Radio-interferometric Imaging of Very Large Objects: Implications for Array Design"*, Astron. Astrophys., **271**, 697.

Cornwell, T.J. 1995, *"The Generic Interferometer: I"*, AIPS++ Implementation Note 183 (Socorro, NM: NRAO)

Cornwell, T.J., Golap, K., & Bhatnagar, S. 2008, *"The Noncoplanar Baselines Effect in Radio Interferometry: The W-Projection Algorithm"*, IEEE Journal of Selected Topics in Signal Processing, **2(5)**, 647

Hamaker, J.P., Bregman, J.D., & Sault, R.J. 1996, *"Understanding Radio Polarimetry. I. Mathematical Foundations"*, Astron. Astrophys. Suppl., **117**, 137

Kemball, A., & Martinsek, A. 2005, *"Bootstrap Resampling as a Tool for Radio Interferometric Imaging Fidelity Assessment"*, Astron. J., **129**, 1760

Middelberg, E. *et al.* 2008, *"Deep Australia Telescope Large Area Survey Radio Observations of the European Large Area ISO Survey S1/Spitzer Wide-area Infrared Extragalactic Field"*, Astron. J., **135**, 1276

Mitchell, D.A., Greenhill, L.J., Wyath, R.B., Sault, R.J., Lonsdale, C.J., Capallo, R.J., Morales, M.F., & Ord, S.M. 2008, *"Real-Time Calibration of the Murchison Widefield Array"*, IEEE Journal of Selected Topics in Signal Processing, **2(5)**, 707

Morales, M. & Matejek, M. 2009, *"Software Holography: Interferometric Data Analysis for the Challenges of Next Generation Observatories"*, submitted, http://adsabs.harvard.edu/abs/2008arXiv0810.5107M

Noordam, J.E. 1995, *"Some Practical Aspects of the Matrix-based Measurement Equation of a Generic Radio Telescope"*, AIPS++ Implementation Note 185 (Socorro, NM:NRAO)

Noordam, J.E. & Smirnov, O.M. 2009, *"MeqTrees: A Software Module for Implementing an Arbitrary Measurement Equation and Solving for its Parameters"*, in preparation, http://www.astron.nl/meqwiki/ReferencePapers?action=AttachFile&do=get&target=reference_paper.pdf

Perley, R.A. 1986, *"High-Fidelity Imaging"*, in Synthesis Imaging: NRAO Summer School 1985 (Green Bank, WV: NRAO), p.161.

Schilizzi, R.T. et al. 2007, *"Preliminary Specifications for the Square Kilometer Array"*, SKA Memo. 100, http://www.skatelescope.org/PDF/memos/100_Memo_Schilizzi.pdf